THE JOURNAL OF PHYSICAL CHEMISTRY C

pubs.acs.org/JPCC

Article

Micro-Defects in Monolayer MoS_2 Studied by Low-Temperature Magneto-Raman Mapping

Yang Yang,* Wuguo Liu, Zhongtao Lin, Ke Zhu, Shibing Tian, Yuan Huang, Changzhi Gu, and Junjie Li*

Cite This: J. Phys. Chem. C 2020, 124, 17418−17422

Read Online

ABSTRACT: In this work, magneto-Raman mapping was performed on monolayer MoS_2 at 4 K, which exhibited a prominent magnetic field-induced modulation of phonon intensity. Interestingly, structural microinhomogeneity in MoS_2 was observed in the mapping images under certain magnetic fields, indicating the existence of lattice defects in monolayer MoS_2. Remarkably, the magneto-optical Raman intensity for the defect zone was only 26% of that for the regular zone, which could be attributed to the scattered electron motion by lattice defects. These results provided a deeper understanding of the mechanisms behind the magneto-optical Raman effects in MoS_2. Moreover, it was demonstrated that the low-temperature magneto-Raman mapping technique could be a highly sensitive tool to directly examine the microstructure in two-dimensional (2D) transition-metal dichalcogenides.

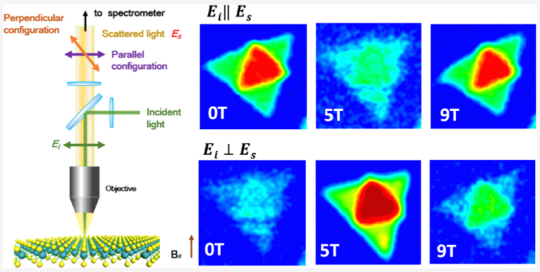

1. INTRODUCTION

Two-dimensional (2D) transition-metal dichalcogenides (TMDs) have attracted extensive interest because of their extraordinary physical properties and widespread applications in optoelectronic devices.[1,2] TMDs have been demonstrated to possess a variety of striking physical properties, such as electron−hole Coulomb interactions,[3] exotic valley physics,[4] and strong spin−orbit coupling.[5,6] Taking advantage of these physical properties, TMDs have been employed as building blocks in spin valleytronics,[7] photodetectors,[8] and ultrashort channel transistors.[9,10]

In recent years, magneto-optical effects in 2D TMDs, such as valley Zeeman splitting,[11,12] valley- and spin-polarized Landau levels,[13] magnetic field-modulated valley polarization, and valley coherence,[14−16] have been studied to further extend the application of TMDs in spintronics and valleytronics. Optical spectroscopic methods, such as circular polarized photoluminescence and magnetic circular dichroism, have been employed in the study of the magneto-optical effects in TMDs.[17−20] Recently, Raman spectroscopy has been demonstrated to be a feasible tool for investigating the magneto-optical effects in 2D TMDs.[21−23] A giant magneto-optical Raman effect was detected in MoS_2 by Ji et al., which was associated with magnetic field-induced symmetry breaking.[21] However, these previous studies were carried out at 77 K and room temperature. Magneto-Raman studies on 2D TMDs at liquid helium temperature (4.2 K) have not been reported. What is more, although the Raman mapping technique has been demonstrated to be a feasible tool to investigate the structural inhomogeneity of TMDs, to our knowledge, it has not been employed to investigate the magneto-optical properties of TMDs on a sub-micrometer scale.

In this work, low-temperature (4 K) polarized Raman mapping was performed on monolayer MoS_2 under different magnetic fields to get a clear overview of the magneto-optical effects in MoS_2. First, polarized Raman mapping images clearly demonstrated the structural microinhomogeneity in monolayer MoS_2, in which a microarea with lattice defects was detected. Then, dramatic magnetic field-induced modifications of the phonon intensity were observed and compared in detail between regular and defective monolayer MoS_2. Our results provide a closer insight into the mechanism of the magneto-optical Raman effects and demonstrate the high sensitivity of the magneto-Raman mapping technique for the examination of the microlattice structure of 2D TMDs.

2. METHODS

Experiments were performed on single-crystalline monolayer and bilayer MoS_2 grown through a chemical vapor deposition (CVD) process on 90 nm SiO_2/Si substrates. Figure 1a shows a white-light micrograph of the sample with thickness overlaid.

Received: June 4, 2020
Revised: July 10, 2020
Published: July 15, 2020

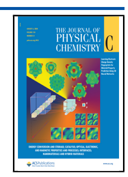

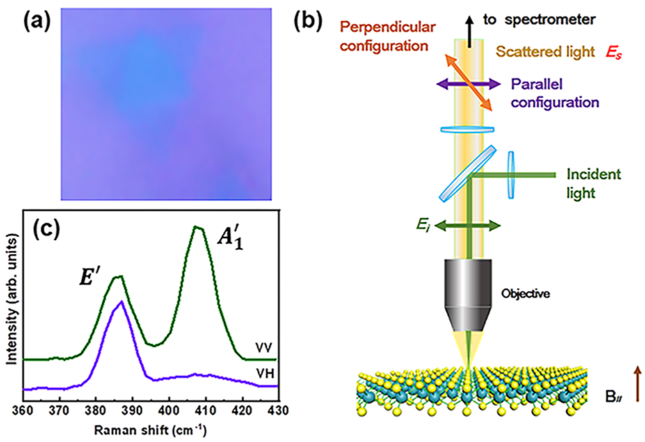

Figure 1. (a) Optical image of the MoS_2 sample used in this work. (b) Schematic of the polarization configurations employed in the magneto-Raman measurements. (c) Polarized Raman spectra of monolayer MoS_2 collected at 4 K.

The number of layers was further confirmed by ultra-low-frequency Raman spectroscopy. The low-temperature magne-to-Raman measurements were performed in a cryostat with a custom-designed confocal micro-Raman spectroscopy/image system. The temperature was fixed at 4 K, while the magnetic field was perpendicular to the sample surface and varied from 0 to 9 T. A linearly polarized 532 nm laser was used as the excitation source, and a beam size of ∼1 μm and a power of ∼4 mW were used to illuminate the sample. The Raman spectra/mapping images were collected in two different polarization configurations: parallel (the polarizations of scattered and incident light are parallel to each other, termed VV) and crossed polarization (the polarization of scattered light is perpendicular to that of incident light, termed VH), as illustrated in Figure 1b. Figure 1c presents the polarized Raman spectra of monolayer MoS_2 collected at 4 K, in which the peaks at around 385 and 408 cm^{-1} exhibit obvious polarization dependence. Because of the discrepancy in the crystalline symmetry between bulk, monolayer, and bilayer MoS_2, the symmetric expressions of these two Raman modes are different. For convenience, these two modes are assigned as E' and A_1' modes, respectively, following the assignment of monolayer MoS_2.[24] As shown in Figure 1c, the E' mode just appears in the VH configuration, whereas the A_1' mode can be seen only in the VV configuration. The Raman spectra of monolayer MoS_2 exhibited good agreement with the Raman selection rules (RSRs).[25,26]

3. RESULTS AND DISCUSSION

First, magnetic field-dependent polarized Raman images were created using the intensity of the A_1' mode because of the strong polarization dependence of the A_1' mode, and are displayed in Figure 2. Triangle-shaped patterns are clearly seen in Figure 2a, in which the monolayer and bilayer MoS_2 can be distinguished easily. Compared with the monolayer MoS_2 area in green, the bilayer MoS_2 area is a red triangle because of the higher Raman intensity due to the doubled thickness. As presented in Figure 2a,f, the 0 T images exhibit clear polarization dependence, similar to the spectra (see Figure 1c). The A_1' mode has a high intensity in the VV configuration, whereas it nearly disappears in the VH configuration. It is noteworthy that with increased magnetic field, the Raman mapping images show opposite evolution in these two polarization configurations. When the magnetic field reaches 5 T, the A_1' mode almost disappears in the VV configuration, whereas it exhibits the highest intensity in the VH configuration. Then, the image recovers with a continuous increase in the magnetic field and resembles the 0 T image features at 9 T. In sharp contrast, the intensity image for the E' mode does not show obvious changes with increasing magnetic field (not shown here).

Interestingly, a yellow spot appears at the bottom corner of the monolayer green triangle at 3 T at VH polarization, as shown in Figure 2g, suggesting the distinct microstructure in this microarea. Remarkably, this cannot be observed in the optical image of the sample (Figure 1a). Furthermore, compared with the green area (G-zone) of the monolayer, the yellow spot (Y-zone) exhibits remarkable polarization dependence.

To gain a deeper insight into the difference between the G-zone and Y-zone monolayer MoS_2, polarized Raman spectra from these two different areas were collected as a function of magnetic field with an increment of 0.5 T. As the E' mode for monolayer MoS_2 is almost magnetic field-independent, all of the spectra were normalized using the intensity of the E' mode to see the variation of the A_1' peak, as presented in Figure 3. As shown in Figure 3a, in the VH configuration, the intensity of the A_1' mode for the G-zone grows with increasing field, reaches the highest value at 5 T, and then recedes with a further increase in field. In sharp contrast, the intensity of the A_1' mode displays inverse trend in the VV polarization

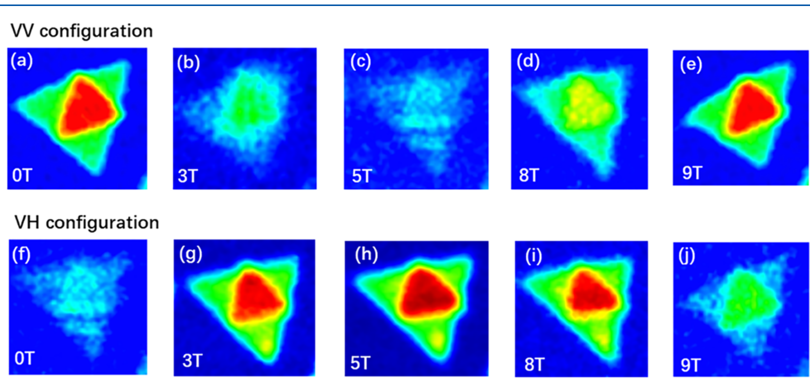

Figure 2. Magnetic field-dependent Raman mapping images created using the intensity of the A_1' mode obtained in the VV configuration (a−e) and the VH configuration (f−j).

https://dx.doi.org/10.1021/acs.jpcc.0c04922
J. Phys. Chem. C 2020, 124, 17418−17422

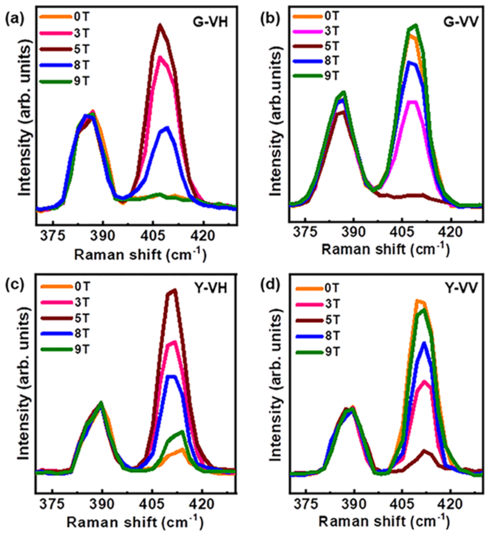

Figure 3. Polarized Raman spectra of (a) and (b) G-zone monolayer MoS_2, and (c) and (d) Y-zone monolayer MoS_2 collected at typical magnetic fields.

configuration (see Figure 3b). The overall magnetic field evolution of the Raman spectra for the Y-zone is similar to that of the G-zone, as exhibited in Figure 3c,d. However, noteworthy distinctions between the Y- and G-zones can be addressed. As shown in Figure 3c, a weak A_1' mode can be seen in the VH configuration at 0 T, which contrasts with that for the G-zone MoS_2. According to RSRs,[27] the A_1' mode is zero in the VH configuration. The leakage of the A_1' mode can be attributed to localized symmetry breaking due to the lattice defects or deformation in the Y-zone. Moreover, the A_1' mode cannot fully disappear in the VV configuration at 5 T due to the breaking of RSRs. In addition, the E' mode also exhibits some differences between the regular and defect areas, although it exists in all polarization configurations and magnetic fields. Taking the VH spectra at 5 T for example, the relative intensity of the E' mode for the defective MoS_2 is lower than that for regular MoS_2, as presented in Figure 3a,c.

Then, the Raman spectra of the G- and Y-zones are deconvoluted using the Lorentzian/Gaussian mixed function, to get a clear view of the intensity modulation under magnetic fields. As presented in Figure 4a, the intensity of the A_1' mode

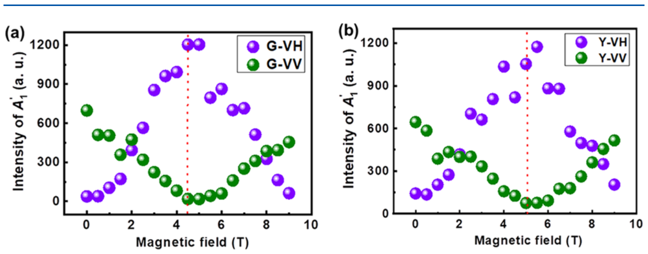

Figure 4. Magnetic field-dependent intensity of the A_1' mode for (a) G-zone and (b) Y-zone in different polarization configurations.

of the G-zone exhibits a magnetic field-induced anticorrelation evolution between the VV and VH configurations. The maximum intensity in the VH configuration and the minimum intensity in the VV configuration are observed at 4.5 T. On the other hand, slightly different from the G-zone, the resonance center for the Y-zone is at around 5 T, as shown in Figure 4b. In sharp contrast, the E' mode does not exhibit clear disciplinary variation under the magnetic field (not shown here).

One can see in Figure 4 that the intensity of the A_1' mode fluctuated slightly, although it has exhibited obvious regularity as a function of the magnetic field. To eliminate the interference due to the intensity fluctuation, the intensity ratio of the A_1' mode to E' mode was calculated as a function of the magnetic field. The E' mode was employed as a reference because it did not exhibit obvious changes under magnetic fields. As presented in Figure 5, the intensity ratio varied

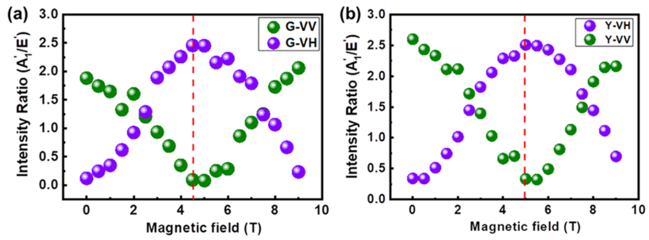

Figure 5. Magnetic field-dependent intensity ratio of the A_1' mode to E' mode for (a) G-zone and (b) Y-zone in different polarization configurations.

smoothly with increased magnetic fields. Moreover, the resonance magnetic field can be seen clearly at 4.5 and 5 T for regular MoS_2 and defective MoS_2, respectively.

The discrepancy in magnetic field dependences between the A_1' and E' modes should be related to their corresponding atomic vibrations. As we know, the A_1' mode originates from the relative vibrations of two S atoms along the out-of-plane direction, whereas the E' mode arises from the in-plane relative vibrations between the Mo and S atoms. Therefore, the A_1' mode is thought to be more sensitive to the magnetic field, which is perpendicular to the MoS_2 flake. As discussed in previous reports, the fluctuation of the Raman intensity was correlated with the magnetic field, which influenced the electrons that mediate the inelastic light scattering, consequently resulting in changes in the second-order electronic susceptibility α.[19] However, we cannot see obvious differences in the magnetic field-dependent intensity of the A_1' mode between the G- and Y-zones.

From the results shown in Figures 4 and 5, one can find that the low-temperature (4 K) magneto-Raman results are significantly different from those in previous reports obtained at higher temperatures (300 K). As reported in ref 21 the resonance field was observed at 7 T, whereas the resonance field in our work is down to 4.5 T. The large discrepancy in resonance field could be attributed to the lower temperature in this work, which can significantly suppress the thermal fluctuation, leading to the prominent improvement of the optical mobility. The resonant magnetic field strength is inversely proportional to the optical mobility,[19,20] so that the resonance field becomes smaller at 4 K.

From the intensity evolution of the magnetic field in Figure 4, we cannot see any significant difference between regular and defective monolayer MoS_2. To quantify the effects of magnetic field on the Raman intensity respons of monolayer MoS_2, the magneto-Raman intensity parameter was calculated according to previous publications as[18,19] magneto-Raman intensity $=\frac{I(B)-I(0)}{I(0)}\times 100\%$ determined from the magnetic field-dependent Raman intensity I(B). As presented in Figure 6a,c, the magneto-Raman intensity of the E' mode is nearly

https://dx.doi.org/10.1021/acs.jpcc.0c04922
J. Phys. Chem. C 2020, 124, 17418−17422

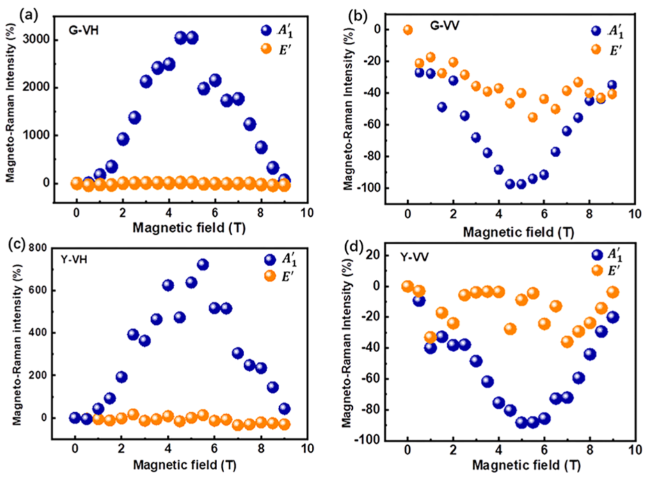

Figure 6. Magneto-Raman intensity for the G-zone obtained in the (a) VH and (b) VV configurations and for the Y-zone collected in the (c) VH and (d) VV configurations. Dark blue and orange symbols represent the A_1' and E' modes, respectively.

zero in the VH configuration. On the other hand, the A_{1g} mode possesses the largest magneto-Raman intensity and can be boosted up to 3000% for the G-zone MoS_2. In sharp contrast, the VH magneto-Raman intensity for the Y-zone is only 800%. Moreover, the VV magneto-Raman intensity of the A_1' mode is negative and could reach −100% at around 4.5 T for the G-zone, whereas it is only −90% at around 5 T for the Y-zone.

The large discrepancy in the magneto-Raman intensity between the G- and Y-zones undoubtedly demonstrates the differences in the magneto-optical effect responses in these two areas. As was reported previously, the modulated Raman signal was proposed to be related to magnetic field-induced electron motion.[21] Therefore, the electron mobility plays a key role in the magneto-Raman intensity of the A_{1g} mode. As reported, point defects are the dominant types of defects in single-crystalline 2D MoS_2, among which the vacancies of S atoms are the prominent defects in mechanically exfoliated and CVD-grown MoS_2.[28,29] The point defects, such as localized disorders, are significant scattering centers of carriers, which can reduce the mobility of charge carriers through the intrinsic conduction or valence band.[26] Therefore, the magneto-Raman intensity in the Y-zone is significantly weakened as a result of the reduced electron mobility. Moreover, the density of point defects in the Y-zone is demonstrated to be much higher than that in the G-zone, which also explains the origin for the leakage of the A_1' mode in the VH configuration. Ghorbani-Asl et al. demonstrated that local defects introduce strongly localized midgap states in the electronic structure that act as scattering centers using the density-functional-based methods.[30] In addition to the reduction of conductivity across the line defects and selected grain boundary models, these isolated scattering states can introduce high anisotropy in quantum conductance. The anisotropy in transport is direction-dependent due to the structural anisotropy of the system, which also plays a role in the breaking of RSRs. Overall, the observations in Figure 6 clearly demonstrate that the magneto-optical Raman effect is authentically associated with electron motion, which is sensitive to the crystalline quality of MoS_2.

4. CONCLUSIONS

To summarize, we have performed a comprehensive magnetic field-dependent Raman spectroscopy investigation on CVD-grown monolayer MoS_2 at 4 K. The structural micro-inhomogeneity of MoS_2 was expressed using polarized Raman mapping under magnetic fields, clearly revealing the existence of lattice defects in the sample. Magnetic field-induced modulations of Raman spectra were observed, in which the A_1' mode exhibited dramatic magneto-optical Raman effects. The discrepancy in the magneto-optical Raman intensity between regular and defective monolayer MoS_2 can be attributed to the impeded electron motion due to the increased grain boundaries and vacancies in the defect zone. Our results demonstrate that the magneto-optical Raman mapping technique is a feasible tool to directly survey the microinhomogeneity in 2D TMDs, providing useful information for their further application in spintronic devices.

■ AUTHOR INFORMATION

Corresponding Authors

Yang Yang − *Beijing National Laboratory for Condensed Matter Physics, Institute of Physics, Chinese Academy of Sciences, Beijing 100190, People's Republic of China;* orcid.org/0000-0003-3785-9233; Email: yang.yang@iphy.ac.cn

Junjie Li − *Beijing National Laboratory for Condensed Matter Physics, Institute of Physics, Chinese Academy of Sciences, Beijing 100190, People's Republic of China; School of Physical Sciences, University of Chinese Academy of Sciences, Beijing 100049, People's Republic of China; Songshan Lake Materials Laboratory, Dongguan, Guangdong 523808, People's Republic of China;* orcid.org/0000-0002-1508-9891; Email: jjli@iphy.ac.cn

Authors

Wuguo Liu − *Beijing National Laboratory for Condensed Matter Physics, Institute of Physics, Chinese Academy of Sciences, Beijing 100190, People's Republic of China*

Zhongtao Lin − *Beijing National Laboratory for Condensed Matter Physics, Institute of Physics, Chinese Academy of Sciences, Beijing 100190, People's Republic of China*

Ke Zhu − *Beijing National Laboratory for Condensed Matter Physics, Institute of Physics, Chinese Academy of Sciences, Beijing 100190, People's Republic of China*

Shibing Tian − *Beijing National Laboratory for Condensed Matter Physics, Institute of Physics, Chinese Academy of Sciences, Beijing 100190, People's Republic of China*

Yuan Huang − *Beijing National Laboratory for Condensed Matter Physics, Institute of Physics, Chinese Academy of Sciences, Beijing 100190, People's Republic of China*

Changzhi Gu − *Beijing National Laboratory for Condensed Matter Physics, Institute of Physics, Chinese Academy of Sciences, Beijing 100190, People's Republic of China; School of Physical Sciences, University of Chinese Academy of Sciences, Beijing 100049, People's Republic of China*

Complete contact information is available at: https://pubs.acs.org/10.1021/acs.jpcc.0c04922

Notes

The authors declare no competing financial interest.

https://dx.doi.org/10.1021/acs.jpcc.0c04922
J. Phys. Chem. C 2020, 124, 17418−17422

■ ACKNOWLEDGMENTS

We thank Dr. Feng Jin for fruitful discussions. This work was supported by the National Key Research and Development Program of China (Grant No. 2018YFB0703500), the National Natural Science Foundation of China (Grant No. 11704401), and the Scientific Equipment Development Project of the Chinese Academy of Sciences (Grant No. YJ-KYYQ20170027).

■ REFERENCES

(1) Zeng, H.; Cui, X. An Optical Spectroscopic Study on Two-Dimensional Group-Vi Transition Metal Dichalcogenides. *Chem. Soc. Rev.* **2015**, *44*, 2629–2642.

(2) Manzeli, S.; Ovchinnikov, D.; Pasquier, D.; Yazyev, O. V.; Kis, A. 2D Transition Metal Dichalcogenides. *Nat. Rev. Mater.* **2017**, *2*, No. 17033.

(3) Mak, K. F.; He, K.; Lee, C.; Lee, G.; Hone, J.; Heinz, T. F.; Shan, J. Tightly Bound Trions in Monolayer MoS_2. *Nat. Mater.* **2013**, *12*, 207–211.

(4) Sie, E. J.; Lui, C. H.; Lee, Y.-H.; Fu, L.; Kong, J.; Gedik, N. Large Valley-Exclusive Bloch-Siegert Shift in Monolayer WS_2. *Science* **2017**, *355*, 1066–1069.

(5) Zhu, Z.; Cheng, Y.; Schwingenschlögl, U. Giant Spin-Orbit-Induced Spin Splitting in Two-Dimensional Transition-Metal Dichalcogenide Semiconductors. *Phys. Rev. B* **2011**, *84*, No. 153402.

(6) Xu, X.; Yao, W.; Xiao, D.; Heinz, T. F. Spin and Pseudospins in Layered Transition Metal Dichalcogenides. *Nat. Phys.* **2014**, *10*, 343–350.

(7) Xiao, D.; Liu, G.-B.; Feng, W.; Xu, X.; Yao, W. Coupled Spin and Valley Physics in Monolayers of MoS_2 and Other Group-Vi Dichalcogenides. *Phys. Rev. Lett.* **2012**, *108*, No. 196802.

(8) Huo, N.; Konstantatos, G. Recent Progress and Future Prospects of 2D-Based Photodetectors. *Adv. Mater.* **2018**, *30*, No. 1801164.

(9) Desai, S. B.; Madhvapathy, S. R.; Sachid, A. B.; Llinas, J. P.; Wang, Q.; Ahn, G. H.; Pitner, G.; Kim, M. J.; Bokor, J.; Hu, C. MoS_2 Transistors with 1-Nanometer Gate Lengths. *Science* **2016**, *354*, 99–102.

(10) Xie, L.; Liao, M.; Wang, S.; Yu, H.; Du, L.; Tang, J.; Zhao, J.; Zhang, J.; Chen, P.; Lu, X.; et al. Graphene-Contacted Ultrashort Channel Monolayer MoS_2 Transistors. *Adv. Mater.* **2017**, *29*, No. 1702522.

(11) Srivastava, A.; Sidler, M.; Allain, A. V.; Lembke, D. S.; Kis, A.; Imamoğlu, A. Valley Zeeman Effect in Elementary Optical Excitations of Monolayer WSe_2. *Nat. Phys.* **2015**, *11*, 141–147.

(12) Aivazian, G.; Gong, Z.; Jones, A. M.; Chu, R.-L.; Yan, J.; Mandrus, D. G.; Zhang, C.; Cobden, D.; Yao, W.; Xu, X. Magnetic Control of Valley Pseudospin in Monolayer WSe_2. *Nat. Phys.* **2015**, *11*, 148–152.

(13) Wang, Z.; Shan, J.; Mak, K. F. Valley-and Spin-Polarized Landau Levels in Monolayer WSe_2. *Nat. Nanotechnol.* **2017**, *12*, 144.

(14) Smoleński, T.; Goryca, M.; Koperski, M.; Faugeras, C.; Kazimierczuk, T.; Bogucki, A.; Nogajewski, K.; Kossacki, P.; Potemski, M. Tuning Valley Polarization in a WSe_2 Monolayer with a Tiny Magnetic Field. *Phys. Rev. X.* **2016**, *6*, No. 021024.

(15) Schmidt, R.; Arora, A.; Plechinger, G.; Nagler, P.; del Águila, A. G.; Ballottin, M. V.; Christianen, P. C.; de Vasconcellos, S. M.; Schüller, C.; Korn, T.; Bratschitsch, R. Magnetic-Field-Induced Rotation of Polarized Light Emission from Monolayer WS_2. *Phys. Rev. Lett.* **2016**, *117*, No. 077402.

(16) Norden, T.; Zhao, C.; Zhang, P.; Sabirianov, R.; Petrou, A.; Zeng, H. Giant Valley Splitting in Monolayer WS_2 by Magnetic Proximity Effect. *Nat. Commun.* **2019**, *10*, No. 4163.

(17) Branny, A.; Wang, G.; Kumar, S.; Robert, C.; Lassagne, B.; Marie, X.; Gerardot, B. D.; Urbaszek, B. Discrete Quantum Dot Like Emitters in Monolayer $MoSe_2$: Spatial Mapping, Magneto-Optics, and Charge Tuning. *Appl. Phys. Lett.* **2016**, *108*, No. 142101.

(18) Kuhnert, J.; Rahimi-Iman, A.; Heimbrodt, W. Magneto Photoluminescence Measurements of Tungsten Disulphide Monolayers. *J. Phys.: Condens. Matter.* **2017**, *29*, No. 08LT02.

(19) Zou, C.; Cong, C.; Shang, J.; Zhao, C.; Eginligil, M.; Wu, L.; Chen, Y.; Zhang, H.; Feng, S.; Zhang, J.; et al. Probing Magnetic-Proximity-Effect Enlarged Valley Splitting in Monolayer WSe_2 by Photoluminescence. *Nano. Res.* **2018**, *11*, 6252–6259.

(20) Wu, Y.; Shen, C.; Tan, Q.; Shi, J.; Liu, X.; Wu, Z.; Zhang, J.; Tan, P.; Zheng, H. Valley Zeeman Splitting of Monolayer MoS_2 Probed by Low-Field Magnetic Circular Dichroism Spectroscopy at Room Temperature. *Appl. Phys. Lett.* **2018**, *112*, No. 153105.

(21) Ji, J.; Zhang, A.; Fan, J.; Li, Y.; Wang, X.; Zhang, J.; Plummer, E.; Zhang, Q. Giant Magneto-Optical Raman Effect in a Layered Transition Metal Compound. *Proc. Nat. Acad. Sci. U.S.A.* **2016**, *113*, 2349–2353.

(22) Du, L.; Zhang, Q.; Gong, B.; Liao, M.; Zhu, J.; Yu, H.; He, R.; Liu, K.; Yang, R.; Shi, D.; et al. Robust Spin-Valley Polarization in Commensurate MoS_2/Graphene Heterostructures. *Phys. Rev. B* **2018**, *97*, No. 115445.

(23) Du, L.; Jia, Z.; Zhang, Q.; Zhang, A.; Zhang, T.; He, R.; Yang, R.; Shi, D.; Yao, Y.; Xiang, J.; et al. Electronic Structure-Dependent Magneto-Optical Raman Effect in Atomically Thin WS_2. *2D Mater.* **2018**, *5*, No. 035028.

(24) Zhang, X.; Qiao, X.-F.; Shi, W.; Wu, J.-B.; Jiang, D.-S.; Tan, P.-H. Phonon and Raman Scattering of Two-Dimensional Transition Metal Dichalcogenides from Monolayer, Multilayer to Bulk Material. *Chem. Soc. Rev.* **2015**, *44*, 2757–2785.

(25) Drapcho, S. G.; Kim, J.; Hong, X.; Jin, C.; Shi, S.; Tongay, S.; Wu, J.; Wang, F. Apparent Breakdown of Raman Selection Rule at Valley Exciton Resonances in Monolayer MoS_2. *Phys.Rev. B* **2017**, *95*, No. 165417.

(26) Kim, H.; Ko, H.; Kim, S. M.; Rho, H. Polarization-Dependent Anisotropic Raman Response of CVD-Grown Vertically Stacked MoS_2 Layers. *J. Raman. Spectrosc.* **2020**, *51*, 774–780.

(27) Loudon, R. The Raman Effect in Crystals. *Adv. Phys.* **1964**, *13*, 423–482.

(28) Santosh, K.; Longo, R. C.; Addou, R.; Wallace, R. M.; Cho, K. Impact of Intrinsic Atomic Defects on the Electronic Structure of MoS_2 Monolayers. *Nanotechnology* **2014**, *25*, No. 375703.

(29) Hong, J.; Hu, Z.; Probert, M.; Li, K.; Lv, D.; Yang, X.; Gu, L.; Mao, N.; Feng, Q.; Xie, L. Exploring Atomic Defects in Molybdenum Disulphide Monolayers. *Nat. Commun.* **2015**, *6*, No. 6293.

(30) Ghorbani-Asl, M.; Enyashin, A. N.; Kuc, A.; Seifert, G.; Heine, T. Defect-Induced Conductivity Anisotropy in MoS_2 Monolayers. *Phys. Rev. B* **2013**, *88*, No. 245440.

https://dx.doi.org/10.1021/acs.jpcc.0c04922
J. Phys. Chem. C 2020, 124, 17418−17422